Plasma Physics and Controlled Fusion

PAPER • **OPEN ACCESS**

Pellet fueling experiments in Wendelstein 7-X

To cite this article: J Baldzuhn *et al* 2019 *Plasma Phys. Control. Fusion* **61** 095012

View the article online for updates and enhancements.

Recent citations

- First results from an event synchronized—high repetition Thomson scattering system at Wendelstein 7-X
H. Damm *et al*

IOP ebooks™

Bringing you innovative digital publishing with leading voices to create your essential collection of books in STEM research.

Start exploring the collection - download the first chapter of every title for free.

This content was downloaded from IP address 129.13.72.195 on 17/12/2019 at 09:46

OPEN ACCESS
IOP Publishing
Plasma Physics and Controlled Fusion
Plasma Phys. Control. Fusion **61** (2019) 095012 (16pp)
https://doi.org/10.1088/1361-6587/ab3567

Pellet fueling experiments in Wendelstein 7-X

J Baldzuhn[1], H Damm[1], C D Beidler[1], K McCarthy[2], N Panadero[2], C Biedermann[1], S A Bozhenkov[1], K J Brunner[1], G Fuchert[1], Y Kazakov[3], M Beurskens[1], M Dibon[4], J Geiger[1], O Grulke[1], U Höfel[1], T Klinger[1], F Köchl[5], J Knauer[1], G Kocsis[6], P Kornejew[1], P T Lang[4], A Langenberg[1], H Laqua[1], N A Pablant[7], E Pasch[1], T S Pedersen[1], B Ploeckl[4], K Rahbarnia[1], G Schlisio[1], E R Scott[1], T Stange[1], A von Stechow[1], T Szepesi[6], Y Turkin[1], F Wagner[1], V Winters[8], G Wurden[9], D Zhang[1] and Wendelstein 7-X Team[10]

[1] Max-Planck Institut fuer Plasmaphysik IPP, D-17491 Greifswald, Germany
[2] Laboratorio Nacional de Fusión, CIEMAT, Madrid, Spain
[3] Laboratory for Plasma Physics, LPP-ERM/KMS, Brussels, Belgium
[4] Max-Planck Institut fuer Plasmaphysik IPP, D-85748 Garching, Germany
[5] Association EURATOM-Ö AW/ATI, Atominstitut TU Wien, A-1020 Vienna, Austria
[6] Wigner Research Centre for Physiks, 1121 Budapest, XII., Hungary
[7] Princeton Plasma Physics Laboratory, PPPL, Princeton, NJ, United States of America
[8] University of Wisconsin-Madison, Madison, WI 53706, United States of America
[9] Los Alamos National Laboratory LANL, Los Alamos, NM 87545, United States of America

E-mail: baldzuhn@ipp.mpg.de

Received 29 April 2019, revised 25 June 2019
Accepted for publication 22 July 2019
Published 13 August 2019

Abstract

During the two most recent experimental campaigns in the advanced stellarator Wendelstein 7-X (W7-X) (Klinger *et al* 2017 *Plasma Phys. Control. Fusion* **59** 014018; Bosch *et al* 2017 *Nucl. Fusion* **57** 116015; Wolf *et al* 2017 *Nucl. Fusion* **57** 102020; Pedersen *et al* 2017 *Phys. Plasmas* **24** 0555030) hydrogen ice pellet injection was performed for the first time. In order to investigate the potential of pellet fueling in W7-X and to study the particle deposition in a large stellarator, a blower-gun system was installed with 40 pellets capability. The experience gained with this system will be used for the specification of a future steady-state pellet injector system. One important motivation for a pellet injector (Dibon 2014 *Master-Thesis* Technical University Munich, Max-Planck Institut IPP) on W7-X is the mitigation of hollow density profiles expected in case of predominant neoclassical transport. For long-pulse operation of up to 30 min, only electron cyclotron resonance heating is available on W7-X. Hence, pellet injection will be the only source for deep particle fueling. Deep particle fueling by pellets in tokamaks is supported by a *grad-B* drift, if the pellets are injected from the magnetic high-field-side. This approach was tested in W7-X, as well. The injection of series of pellets was also tested. Here, deep fueling is supported for later pellets in the series by the plasma cooling following the initial pellets in the same series. As in earlier experiments in the heliotron LHD (Takeiri *et al* 2017 *Nucl. Fusion* **57** 102023), deep and rapid fueling could be achieved successfully in W7-X.

[10] T Klinger *et al* 2019 *Nucl. Fusion* (https://doi.org/10.1088/1741-4326/ab03a7)

Original content from this work may be used under the terms of the Creative Commons Attribution 3.0 licence. Any further distribution of this work must maintain attribution to the author(s) and the title of the work, journal citation and DOI.

 © Max-Planck-Institut fuer Plasmaphysik Printed in the UK

Keywords: ice pellet injection, central particle fueling, particle transport in an advanced stellarator

(Some figures may appear in colour only in the online journal)

1. Introduction

The stellarator W7-X has been designed to demonstrate the feasibility of an optimized magnetic configuration [1], with a neoclassical energy transport level comparable to axisymmetric fusion devices. Optimized neoclassical particle transport, however, was not included in this concept. Strong coupling that occurs between energy and particle transport in neoclassical theory is expected to cause density control issues [2]. This holds in particular for enhanced central microwave heating by ECRH, which is the principal heating method for W7-X, for which neoclassical calculations predict a scenario of peaked temperature profiles. Hence, the off-diagonal term (thermo-diffusion) driven by the temperature gradient can induce a significant outward particle flux. Hollow density profiles could be the consequence [3], with similarly flat or even hollow pressure profiles. Thus, de-stabilization of MHD modes, in particular the resistive interchange [4] is expected to result in degraded confinement.

ASTRA code [5] calculations predict the need for a central particle fueling rate in the order of $10^{21}\ \mathrm{s}^{-1}$ for 10 MW ECRH heating power. The issue could be further aggravated, if no significant contribution from anomalous particle transport is present, in particular in the bulk plasma. Hence, a neoclassical particle transport barrier in the gradient region might lead to the loss of density control. This holds in particular if the main particle sources are situated at the plasma edge. Central particle fueling by pellet injection can mitigate such a scenario.

W7-X, as a superconducting machine, provides the potential to fully exploit the steady-state capabilities of a stellarator. Therefore, steady-state central particle fueling by pellet injection will be a crucial pre-requisite to maintain that beneficial property. Moreover, stellarators do not suffer from a Greenwald density limit [6]. Hence, the achievement of conditions for a burning fusion plasma could be attained not only by high enough plasma temperatures, but also by plasma densities well above those obtainable in tokamaks of comparable machine size. This approach is encouraged by the empirical International Stellarator Scaling law ISS04 [7]. It comprises a positive electron density, n_e, scaling for the global energy confinement time τ_E proportional to $n_\mathrm{e}^{0.54}$. Therefore, enhanced fueling of W7-X with pellets will always be beneficial, both for sustaining stable and high values of n_e, as well as for maximizing the energy confinement time. Both quantities enter directly the fusion triple product. Even when considering the tokamak Greenwald density limit as an edge density limit, pellet fueling is a powerful core particle source that allows the central density to rise above the Greenwald limit while keeping the edge density low enough to avoid losses of the global confinement, as demonstrated in the tokamak ASDEX Upgrade [8].

Cryogenic pellet experiments, performed with a refurbished blower-gun type injector, have given us a first insight into the interaction of pellets with W7-X plasmas. These same injections have provided a first understanding of the requirements for a future steady-state pellet injector, which will be needed to meet the challenge of continuous fueling in this large machine. Although the sustained mitigation of flat or hollow density profiles has still to be demonstrated, the W7-X discharges available permit initial tackling of the issues of central particle fueling, the choice of the proper injection geometry and the question of efficiency of a series of pellets. For instance, in the case of injection geometry, strongly enhanced central particle deposition is observed in tokamaks when pellets are injected from the magnetic high-field side (HFS) [9]. Inboard launching takes advantage of the *grad-B* induced vertical charge separation in the ablation cloud, leading to a subsequent $E\times B$ drift acceleration of the ionized pellet material that is always directed away from the major machine axis. The considerable increase in pellet fueling efficiency, compared to the low-field side (LFS), makes this technique also interesting for stellarators. However, throughout the two last experimental campaigns, strongly hollow density profiles, or hollow pressure profiles were never observed, neither with pellet injection nor without. Therefore, no vital importance of central particle fueling was given, so far. In section 3, the definition of the fueling efficiency is given.

To make a direct comparison between HFS and LFS in W7-X, two pellet guiding tubes were installed and pellets were injected from both the inboard and outboard sides into the same discharge. However, the *grad-B* effect is expected to be less pronounced compared to a tokamak because *grad-B* is only $0.8\ \mathrm{T\,m^{-1}}$ in W7-X, and therefore smaller than the typical $2\ \mathrm{T\,m^{-1}}$ on the inboard side of a tokamak of comparable minor radius.

Significant progress has also been made to simulated pellet injections into W7-X. This has been done using the Hydrogen Pellet Injection 2 code (HPI2) [10]. Originally developed for tokamaks, HPI2 was recently modified for the use on W7-X [11], i.e. compared to the simple axisymmetric tokamak magnetic topology, the more complex 3D topology of W7-X had to be taken into account. The HPI2 code calculates self-consistently the ablation phase of pellet material, while also taking into account the subsequent perpendicular *grad-B* plasmoid drift. The plasmoid is a high-beta plasma cloud produced by ablation of the cold pellet particles, which are deposited within a single magnetic flux tube. Drift minimizing parallel electrical currents within and outside the

plasmoid are calculated in order to predict the drift damping of the plasmoid. Thus, the effective size of the *grad-B* term, i.e. the plasmoid drift accelaration is a function of the toroidal co-ordinate of W7-X. The resultant pellet deposition calculations obtained with HPI2 were promising, in particular for HFS injection. For instance, calculations predict a much higher fueling efficiency for the HFS case (up to 98%) compared to about 50% for LFS.

As the plasmas during the last two campaigns were heated almost exclusively with ECRH, a possible enhanced ablation of the pellet material by supra-thermal electrons has to be considered because such electrons can be induced by ECR heating. The importance of an enhanced ablation effect is that it can reduce the ice penetration depth into the plasma, thereby leading to reduced fueling efficiencies.

The injection of series of pellets with high repetition frequency results in a pre-cooling of the plasma edge. Initial pellets in the series will thus facilitate deeper penetration for later pellets. To confirm (or disprove) the possibility of improved fueling with series of pellets, experiments in the heliotron LHD were performed [12] before the pellet campaigns on W7-X. Series of pellets were injected into LHD discharges for a range of pellet repetition frequencies, plasma heating methods, pellet ice isotopes and positions of the major plasma axis. The results confirm that the fueling efficiency can be enhanced using series of pellets. The mentioned boundary conditions, like the ice isotope or the location of the major axis played only a minor role for that process. However, if the number of pellets exceeded an upper limit, it became, in some cases, difficult to sustain stable plasma conditions. In a very few cases, a fast central density increase could be observed after the series of pellets, with a rapid change from a more hollow to a more peaked density profile shape. The time constant for this change in profile shape are shorter than the particle diffusion time-scale. The findings from the LHD are compared briefly to the results from W7-X

This paper is organized as follows: in the 'Experimental' section, the stellarator W7-X, the blower-gun and the pellet guide tubes are briefly described, as well as some of the diagnostics used for pellet analysis. In the 'Results' section some of the experimental findings are summarized, with focus on the capabilities of the present system for deep particle fueling, the comparison between LFS and HFS injections, and the potential of series of pellets to achieve deep fueling. In the 'Discussion, outlook' section the experimental results are briefly discussed, with emphasis on the lessons learned for the steady-state injector.

2. Experimental

2.1. The stellarator W7-X

The stellarator W7-X [13–16] provides a toroidal plasma with an effective minor plasma radius of about 0.5 m and a major machine radius of 5.5 m. A set of 70 superconducting coils produces a steady-state magnetic field with a flux density of up to 3 T on the magnetic axis. Always 10 coils are connected in a series, the current in each of the 7 series can be chosen independently from the others. The modular arrangement of the superconducting coils allows for high flexibility concerning the magnetic configuration. At present, ECR heating, with a nominal input power of up to 8 MW and resonant frequency of 140 GHz, is installed for second harmonic heating. Rotatable ECRH launch mirrors allow to choose the radial localization of the heating power focus in the plasma (on- or off-axis). In addition, the polarization of the incident waves can be varied between X2 and O2 orientation [17]. In order to avoid damage to in-vessel installations when the plasma density approaches the cut-off value ($1.2 \times 10^{20}\,\mathrm{m}^{-3}$), a system of microwave sniffer probes monitors the power level of any in-vessel stray-radiation. Recently, two sources for neutral beam injection (NBI) heating systems went into test operation with nominally 4 MW heating power at 55 kV beam energy (full energy beam component). While the ECRH is steady-state capable, the NBI can provide pulse lengths of up to 5 s.

The entire W7-X facility is dedicated to long-pulse operation. Up to 30 min pulse length will be possible when its water-cooled divertors are installed before the next experimental campaign (OP2). During the most recent campaign, intertially cooled divertors were installed in order to investigate the divertor performance and to test the safe exploration of the operational space. During the last two campaigns, the plasma working gas was helium or hydrogen, the pellets were always made of hydrogen ice.

The edge rotational transform of W7-X is suited for open island divertor operation [18] and can be varied between $5/6$ and $5/4$. The standard case iota $\iota \approx 1.0$ is characterized by a chain of 5 magnetic islands surrounding the plasma, according to the $m = 5$ fold toroidal stellarator symmetry of W7-X. Pellet experiments during the most two recent campaigns were performed with four different magnetic configurations. The modular coil set of W7-X, with a combination of non-planar and planar coils, provides the freedom to modify the value of ι, the effective magnetic mirror and ripple, and the horizontal plasma shift. For the pellet experiments, three edge ι values were realized with $\iota(a) \approx 5/4$, $5/5$ and $5/6$, as well as a high-mirror configuration.

2.2. The blower-gun

For pellet injection, a refurbished blower-gun system is installed that can provide pellet series of up to 40 cylindrical hydrogen pellets with a length and diameter of 2 mm and a velocity of up to $250\,\mathrm{m\,s}^{-1}$. Nominally, each pellet contains 3.3×10^{20} hydrogen atoms. Liquid helium is used to cool the cryostat. Pellet acceleration is achieved using helium propellant gas with 2 bar pressure, and the pellet repetition frequency is variable between 2 Hz and 30 Hz. Prior to injection an ice rod with a typical length of 80 mm is frozen out in the extrusion cryostat, from which it is transferred by a stepping motor, in steps of 2 mm, towards a cutting device, the shuttle. The shuttle cuts the individual pellets out of the rod and shifts

them forward to two fast propellant gas valves, where these are accelerated alternatively into two independent guide tubes. Hence, the maximum repetition frequency in each guide tube is 15 Hz. One guide tube ends at the LFS port (labeled AEK41), the other one at the HFS port (labeled AEL41). As the freezing of one single ice rod requires roughly 3 min, the system can not be reloaded during one discharge in W7-X. Typically, the pellet speed was between 170 and 230 m s^{-1}.

The blower-gun was originally built for, and operated on, the tokamak ASDEX-Upgrade [19]. For the operation on W7-X some modifications were necessary. The above described installation of two internal guide tubes allows to feed pellets to the HFS and LFS simultaneously. The injector is foreseen originally for the injection of deuterium pellets, however W7-X operation is currently restricted to hydrogen. To meet the more critical requirements for hydrogen pellet formation compared to those for deuterium, the vacuum pumping efficiency was enhanced considerably (five instead of three turbo-molecular pumps with a pumping speed of 360 l s^{-1} each, and roughing pumps with 620 $m^3 h^{-1}$ pumping speed instead of 90 $m^3 h^{-1}$), before the blower-gun could be operated on W7-X. The reason for this is the lower sublimation temperature for hydrogen (13.9 K) compared to that for deuterium (18.6 K), under vacuum conditions. Another challenge is the reduced breaking stress of hydrogen ice compared to deuterium, making the transfer in a curved guide tube more demanding.

Because of limited space in the torus hall, the injector is situated outside the torus hall, beyond the radiation protection wall. The steel tubes that form the guide tubes have inner and outer diameters of 8 mm and 10 mm, hence the conductance of residual gas is low enough to de-couple W7-X from the blower-gun. These tubes are at ambient temperature. As the distance between the blower-gun and W7-X is too long for a single piece of tube, they are assembled by shorter pieces with maximum 4 m length. The individual pieces are connected by vacuum tight conflat flanges.

In each guide tube a microwave mass detector is installed [20]. They allow for the measurement of the pellet mass and velocity in flight. These residual pellet masses provide directly a measure for pellet erosion along the guide tubes. The detectors utilize the de-tuning of a microwave cavity by the pellet mass once these fly through the cavity. As the detector electronics is sensitive to the magnetic stray field of W7-X, they had to be situated 4 m away from the superconducting coils. The total lengths for the LFS and HFS tubes are 14.5 m and 29.0 m respectively. The distance, measured along the tubes, between the microwave systems and the ports of W7-X is 3.9 m for LFS and 10.3 m for HFS. In order to estimate the pellet erosion for the full tube lengths, it has to be assumed that the erosion rate is similar for both the HFS and LFS tube, and before and after the microwave detectors. When leaving the guide tubes, the pellets have typical masses of 2.0×10^{20} (LFS) and 0.9×10^{20} (HFS) hydrogen atoms, respectively. Each pellet provides a radially averaged plasma density increase of $< 8.0 \times 10^{18}\,m^{-3}$ (LFS) and $< 3.8 \times 10^{18}\,m^{-3}$ (HFS), respectively. Smaller pellets and, hence, smaller density increase can result from a variation of the erosion in the guide tubes from pellet to pellet, poor ice quality or broken pellets.

Two pumping stations with drag turbo pumps (with 80 l s^{-1} pumping speed each) and dry scroll forepumps (with 5 $m^3 h^{-1}$ pumping speed each) evacuate the guide tubes and pump away the hydrogen gas that is released from the pellet ice after contact with the wall of the guide tubes. The drag turbo pumps are also sensitive to the magnetic field, therefore they were installed at the locations of the microwave detectors. In this way the two functionalities of gas pumping and pellet mass measurement could be combined in one device. Gate valves allow separating the guide tube vacuum from the W7-X vessel vacuum. Thus, by closing one of these vacuum gate valves, pellet injection from only one side can be performed. Figure 1 shows a rough sketch of the arrangement. The guide tubes end about 2.5 m away from the last closed flux surface. Then the pellets fly free within the W7-ports, which have an inner diameter of about 400 mm. The pellets show an angular scatter of about $\pm 5°$ in free flight after leaving the guide tube. Therefore, the position of entering the plasma varies by typically about 300 mm, both in toroidal and poloidal direction. The variety in pellet speed, pellet size and entering position might explain, to some extent, the scatter in the observed data,which we will see later.

A large risk for the pellet integrity arises from the long and curved HFS tube that includes S-bends. Since the bending radius of these tubes is 1000 mm in all bends, relatively slow pellet velocities are needed. Larger radii could not be realized because of the very restricted space in vicinity to W7-X. Nevertheless, great care was taken in choosing of the pathway in the torus hall, and the geometrical layout of the HFS guide tube in order to minimize pellet mass loss by erosion in the guide tube. The LFS guide tube is less critical since it is shorter and almost completely straight. Figure 2 shows the geometrical arrangement of the two guide tubes, together with the locations of the microwave systems and the W7-X gate valves. Figure 3 shows the plasma poloidal cross section where the pellets (LFS and HFS) enter the plasma. Both injection ports are slightly inclined with respect to the horizontal plane. The pellet injection geometry at the ports is adapted such that the pellet's flight path points towards the plasma center.

The HFS experiments could be performed in this particular guide tube geometry and into this injection port AEL41 only during the last two campaigns. The present space for the HFS guide tube will be occupied in the next campaign by water-cooling circuits, required to cool the divertor. Computer aided design studies show that an alternative routing for a possible future HFS guide tube will be hindered by enormous technical challenges. It was therefore decided to realize an alternative HFS injection geometry only for the case where HFS fueling efficiency is considerably higher than that for the LFS.

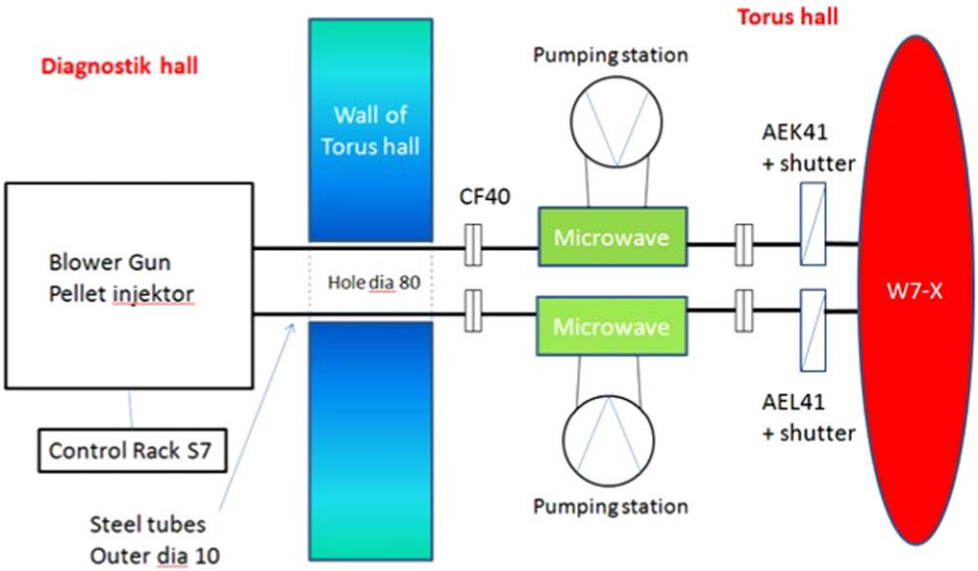

Figure 1. Sketch showing the installation of the blower-gun in the diagnostics hall adjacent to the W7-X torus hall. The halls are separated by a 1.8 m thick concrete wall. The two guide tubes with an outer diameter (dia) of 10 mm (horizontal black lines) pass through a hole in the wall of the torus hall to W7-X with 80 mm diameter. Because of the length of these tubes, shorter pieces with a length between 3 and 5 m are connected together by Conflat CF40 vacuum flanges. Four of these flanges are shown. Also shown are the two microwave systems, drag turbo pumping stations and the two gate valves at the two pellet entrance ports AEK41 (LFS) and AEL41 (HFS). Not to scale.

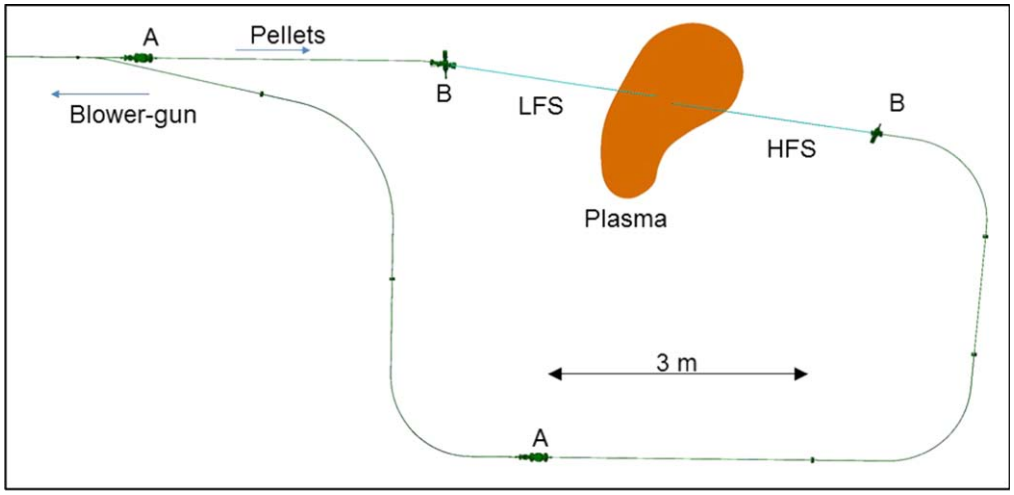

Figure 2. Geometrical shapes of the guide tubes. The pellets enter the tubes from the left (the blower-gun is not shown), the labels A indicate the microwave systems and the localization of the drag turbo-molecular pumps, labels B the gate valves between the guide tubes and the W7-X vessel. W7-X itself is not shown, the plasma shape is roughly approximated. The scale of 3 m shows the size of the arrangement.

2.3. The diagnostics

A fast PIN-photodiode with a bandwidth of 1 MHz records the pellet ablation light, while a standard CMOS video camera registers the ablation cloud in the plasma from behind with 25 Hz frame-rate. Both, photodiode and video camera, can observe LFS and HFS pellets.

In addition, highly sensitive survey cameras view the ablation cloud from the sides: two opposite tangential ports (AEQ41, AEQ50) are used to observe the poloidal cross section of the pellet injection. In the AEQ50 port an EDICAM system [21] using 1.3 Mpixel CMOS cameras normally operates at a 100 Hz or 200 Hz frame-rate. It provides survey pictures of the pellet traces plus the surrounding in-vessel components. The EDICAM system is used without interference filters in front. Figure 4 shows an example of such a long exposure snapshot with two pellets, one LFS and one HFS, which fall by chance into one exposure time interval. Some typical features for pellet injection are highlighted. In parallel to the slow framing mode, the EDICAM system can also record smaller regions of interest (ROIs) with a frame-rate up to 10 kHz. In the port AEQ41, the standard EDICAM system was replaced by an image fiber being relayed to a Photron SA5 fast framing camera, which allows for frame rates up to 350 kHz, but only for a small ROI which is dedicated to detect the pellet ablation region. Due to the short exposure time, the flight path of the

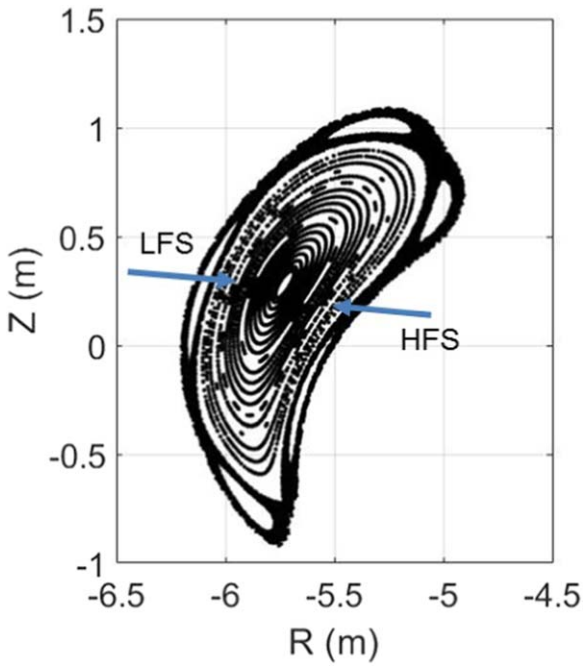

Figure 3. Poloidal cross section just between the two pellet entrance planes at phi = 20° as Poincaré plot. The plot shows the core plasma, the projection of the pellet flight paths into this plane and the 5/5 island chain for the standard magnetic configuration, calculated for plasma beta = 0.

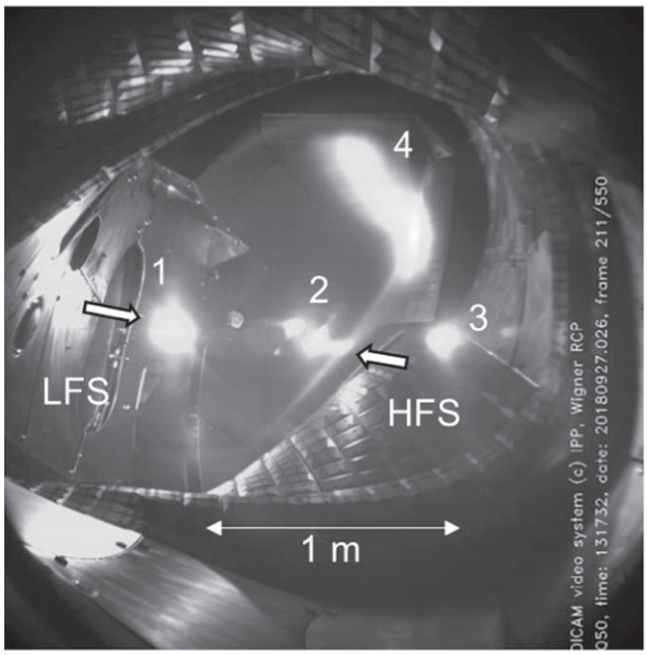

Figure 4. EDICAM image of two pellet ablation clouds that enter the plasma simultaneously. The LFS pellet enters from the left, the HFS pellet from the right, the path of flight is indicated by white arrows. The feature 1 and 2 are the ablation clouds, 3 is a reflection on the vacuum window, 4 is light from the upper divertor chamber. The scale length of 1 m holds for the plane where the pellets enter the plasma. The camera sensitivity is tuned for the observation of vessel wall details, hence the pellet ablation traces are strongly over-exposed.

pellets can be traced quite well since over-exposure effects, that occur with the 'slow' camera system, are avoided. The fast camera is equipped with an interference filter changer for wavelength selection.

The W7-X Thomson scattering system permits the radial measurement of electron density and temperature profiles either with a constant laser repetition frequency, between 5 and 30 Hz. In the burst-mode for fast events [22–24], up to 12 Thomson profiles can be measured with 100 μs temporal separation immediately after a pellet reaches the plasma edge. The proof-of-principle for the burst-mode operation mode was demonstrated in the second part of the most recent operation campaign (OP1.2b), while first pellet data were obtained during the first part of the same campaign (OP1.2a). The burst-mode results will be published in the future.

Magnetic field line tracing calculations [25] have shown that the magnetic flux tube, which is filled by HFS pellet particles, is connected along the magnetic field lines after only 1/5 toroidal transit to the vicinity of the Thomson laser chord on the inboard plane. Therefore, it is expected that the parallel expansion of the pellet material (and the parallel electron cooling) will be detectable after a short delay by the Thomson scattering system. This delay is dominated by the parallel ion sound velocity for the particle cloud expansion along the magnetic field, and the electron thermal velocity for the cooling front. However, in the case of LFS injections, the same tracing calculations predict longer relative distances, so a similar insight is not possible.

Electron temperature profiles are also measured by an electron cyclotron emission system [26]. Radial profiles of the ion temperatures, T_i, and the radial electric field, E_r, are measured by a vacuum ultraviolet spectroscopic system [27], using the x-ray line emission of highly ionized argon lines with an imaging crystal spectrometer. The line integrated electron density is measured by a single line-of-sight dispersion interferometer [28]. Its measurement branch through the plasma lies parallel to the Thomson laser chord, at a nominal distance of $\approx$ 3–5 cm (in real space). No multi-channel interferometer system is available. Plasma impurity radiation is measured using a bolometer camera system with two independent cameras, which allow for the measurement of spatially resolved radiation profiles [29]. Hydrogen wall recycling fluxes are observed by a filterscope-system [30], consisting of multiple sight lines. Several impurity spectral lines coming from the edge can be measured with it, as well as Balmer-alpha light.

2.4. Boundary conditions for pellet experimental sizes and velocities

During the preparation phase for pellet injection it was considered prudent to perform the first pellet experiments in W7-X with conservative sized pellets in order avoid over-fueling the plasma. This point is crucial given that the 140 GHz ECRH in X2-polarization heating has an upper cut-off density of $1.2 \times 10^{20}\,\mathrm{m}^{-3}$. As it was not clear, at which radial positions the initial particle deposition would occur directly after pellet ablation, the risk of local cut-off could not be excluded. To provide access to higher densities in W7-X,

O2-mode heating was tested successfully, this having an upper cut-off density of $2.4 \times 10^{20}\,\mathrm{m}^{-3}$. However, O2 single pass absorption depends strongly on the electron temperature, T_e, and is predicted to drop considerably for T_e values below $\approx$ 2–3 keV. Therefore, the most prominent risk with pellet injection during O2 heating is excess plasma cooling, which is also minimized if the pellets are not too large.

In practice, a maximum of about 7 MW of ECR heating power was available during the OP1.2 campaign for a plasma volume of about 30 m^3. Given the low heating power density, all pellet experiments at densities above $10^{20}\,\mathrm{m}^{-3}$ suffered from T_e values close to this critical value and are thus difficult to conduct. In addition, the low single-pass absorption of O2 mode heating, compared to X2, makes energy confinement studies difficult because an unknown amount of the heating power will be lost as stray radiation. The choice of 2 mm sized pellets was therefore considered a good compromise to promote deep fueling on the one hand, and to reduce the risk of a cut-off or too low T_e on the other.

Due to the rather crowded space situation in the vicinity of the W7-X, it was a challenge to find a pathway for the HFS guide tube that combines sufficiently large bending radii, accessible W7-X ports close to the injector position, a minimum of S-bends and a minimum travel distance for the pellets within the guide tube. These limitations require, in practice, low pellet velocities.

An important property of the blower-gun is its capability to inject series of pellets. The technique of deep particle fueling with series of pellets was tested successfully on LHD [31]. As the experiments in LHD confirmed the validity of that approach, such pellet experiments were performed in W7-X to confirm that finding. In particular the rapid change of the density profile shape from hollow to peaked, as described in [31], requires more attention and has to be reproduced, as it combines the requirements of high fueling efficiency with central particle fueling.

As the W7-X blower-gun is suited principally for injecting series of pellets, rather than for single pellets, pellet series are injected for all experiments. The length of each series varies between 5 and 35 pellets. After initial attempts with small numbers of pellets, it was determined that larger numbers of pellets are more beneficial for density built-up and energy confinement of the discharges.

The pellet team of the tokamak ASDEX-Upgrade provided us with their blower-gun injector [32] and it was found to combine all required specified values summarized above. After a thorough characterization of the as-built properties of that injector, it was shipped to W7-X and installed on site. In the middle of September, 2017, first pellet experiments started.

3. Results

3.1. Pellet penetration and fueling efficiencies

During the OP1.2 experimental campaigns on W7-X, a total of 147 discharges were fueled with pellets, 143 of them having pure ECRH. Roughly 50% of all pellets accelerated from the blower-gun reached the plasma and induced an increase of the electron density. In the case of HFS, the longer guide tube results in higher ice erosion and smaller pellets. Typically, the pellets ablated within about 5–15 cm in real space after they entered the last closed flux surface, corresponding to about 15%–40% of the minor plasma radius, when taking the local flux compression into account. Within the magnetic islands in W7-X, no ablation light intensity could be recorded, neither with the fast PIN photodiode nor with the tangentially observing cameras. Typically, the pellet ablation phase lasts between 0.5 and 1.0 ms.

Finally, since only four discharges were performed with a combination of 5 MW ECRH and NBI heating plus pellets, the database is too poor to draw conclusions with regard to how the heating method impacts on pellet ablation. Nonetheless, from the data available, first observations of the ablation light trace and pellet penetration depth show no significant impact from fast ions originating from the NBI. The same holds for the pellet fueling efficiency.

Pellet fueling efficiency is an important number for assessing fueling characteristics. The fueling efficiency is calculated from the line integrated interferometer measurement of the electron density. The measured line density is divided by the effective interferometer arm length within the plasma (typically $\approx$ 1.3 m), then it is multiplied by an effective plasma volume (typically $\approx$ 24 m^3). This effective plasma volume V_{eff} is determined taking into account the density profile shapes from Thomson scattering for the particular discharge as follows. The profiles are typically flat within effective minor plasma radii $\approx$ 0.4 m, with a density gradient between this location and the effective minor plasma radius a. The total plasma volume within a is typically $\approx$ 32 m^3. The effective minor radius r_1 at $0.5 * n_e(0)$ is taken from $n_e(r)$ to calculate $V_{\mathrm{eff}} = 2 * \pi * R * \pi * r_1^2$ with R being the nominal major plasma radius = 5.5 m. This rough procedure is necessary, because in general no Thomson profiles are available just before and after each pellet (i.e. within a time period <1 ms before and after each pellet) and no multichannel interferometer exists. Therefore, the last available Thomson profile prior to the series of pellets is used for the determination of V_{eff}, and it has to be assumed that the density profile shape does not change considerably during the series of pellets. The video camera data and the fast photodiode indicate that no pellet particles are deposited outside the last closed flux surface. Therefore, we have to assume that all pellet particles that reach the last closed flux surface will contribute to the density increase inside.

For the evaluation of the density jump by the pellets, the difference of the line density measurement 1 ms before and 1 ms after the pellet is used. This provides the difference in electron content in the plasma, yielded exclusively by the pellet. The fueling efficiency is then calculated as the change of number of plasma electrons divided by the electrons provided by the pellet. The latter is taken from the pellet mass measurement by the microwave systems. The dominating uncertainties for this procedure arise from the assumption of constant pellet erosion in the guide tube and the subsequent

evaluation of the pellet mass, being in the range of ±30%. Furthermore, the rough procedure for the estimation for V_{eff}, as described above, will also contribute to the uncertainty.

Fast changes of the wall recycling fluxes in the very moment of the pellet ablation, however, cannot be taken into account by this method. The quantitative estimate of fueling by a transient change of the wall recycling fluxes would make the measurement of these fluxes necessary, integrated over the entire W7-X vessel wall. Such a measurement is presently not available. Thus, we have to assume that the recycling coefficient is constant in the moment of the pellet ablation. Between individual pellets, the wall recycling fluxes could also be affected by the change of the plasma edge density and temperature, induced by the pellets itself. As we evaluate the change in line density only immediately before and after the pellet ablation, the impact of this error source is minimized, however not zero.

The experimental determination of the efficiency can, in addition, be perturbed by unknown particle sources, which depend in a complicated manner on the discharge history during an experimental day, the particle recycling properties of the vessel wall, and/or the gas fueling program. Nonetheless, a particular feature could be observed in a couple of discharges. This is the variation of the pellet fueling efficiency along a series of pellets.

Figure 5 shows the time traces for a discharge with a series of 22 pellets. This discharge combines some typical features observed after pellet injection. Frequently, a transient peaking of the density profile shape can be observed during the phase with pellets. The series of pellets is concluded by a phase with enhanced energy confinement and increased central electron and ion temperatures. Transiently, the energy confinement time exceeds the ISS04 prediction by more than 30%. The peaked density profiles are supported by the central pellet fueling, the good energy confinement by comparably low plasma radiation. During the phase with good energy confinement, the total plasma radiation is lower than comparable discharges fueled by gas puff. This discharge is chosen because the external gas feed is set to zero so the only particle sources are the pellets and the wall recycling flux. During the discharge phases without pellets, i.e. the 5 s before and the 3 s after, the line density remains constant. Hence it can be inferred that the wall recycling fluxes play only a minor role for the fueling, so the density rise is due exclusively to the pellets. The wall recycling coefficient is $R = 1$, i.e. the particle losses from the plasma are compensated by the recycling influx.

Figure 6 shows the fueling efficiencies for the 12 pellets injected into discharge 20180808.009. The upper plot shows the fueling efficiency as a function of the individual pellet number within the series, while the lower plot shows the pellet ablation time, determined from the PIN photodiode and normalized to the pellet mass. The normalization is done to take into account the slightly different pellet masses within the series. It should be noted that all pellets are from the LFS. To guide the eye, fitted curves to the measured data are plotted as well. In the plot, the efficiency of the first pellets is

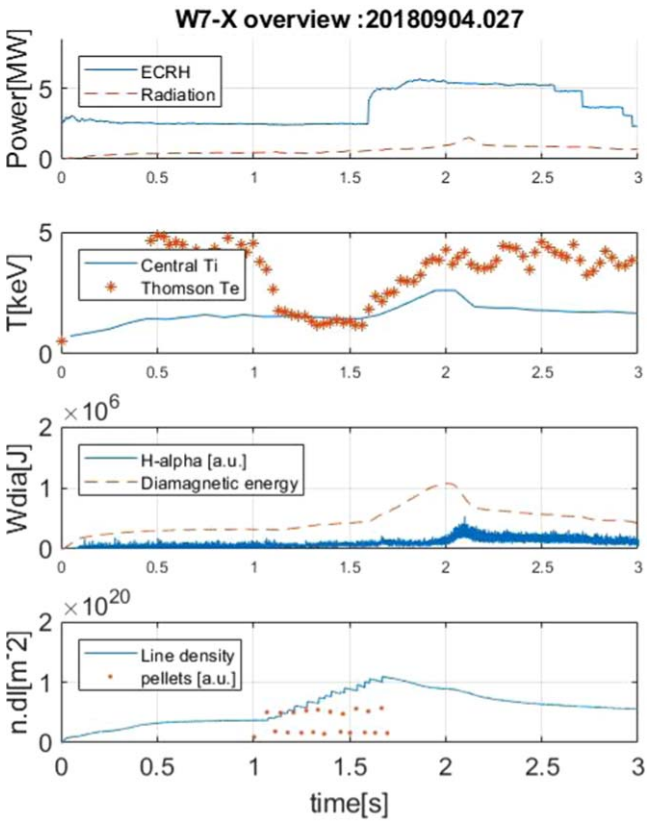

Figure 5. Overview time traces for discharge 20180904.027 with pellets. The first plot shows the ECRH heating power (solid line) and the integrated radiation losses measured by bolometry (dashed line). The second plot shows the central T_{i} (solid line), and the central Thomson T_{e} (stars). The third plot shows the signal of one horizontal H-alpha channel (solid line) and the diamagnetic energy content (dashed line). The fourth plot shows the interferometer line density (solid line) and the injection times for the pellets (dots). Each dot represents one pellet, the height of the dot above the *x*-axis is proportional to the pellet mass.

about 40%. This increases to almost 80% for the pellet number 7–10, before dropping thereafter. This behavior is interpreted as the effect of the pre-cooling of the plasma by first pellets in the series. The length of the pellet ablation time increases gradually during the series, probably as a result of the gradually decreasing electron temperature, as the ablation rate is most sensitive to T_{e}. This points to a gradually increasing pellet penetration depth during the series, which varies in this case between 9 cm for the first pellet and 13 cm (in real space) for the last (pellet number 12), when the measured pellet velocity of about 200 m s^{-1} is taken into account. Here it is assumed that the pellets trace straight lines towards the plasma center, and that pellets do not suffer acceleration or deceleration. So far, we have no good explanation for the drop in fueling efficiency for the last pellets in the series. We can only speculate that the increasing edge density gradient during the series of pellets induces an increasing outward directed diffusive particle flux, which overrules the beneficial deep particle deposition by pellets at the end of the series.

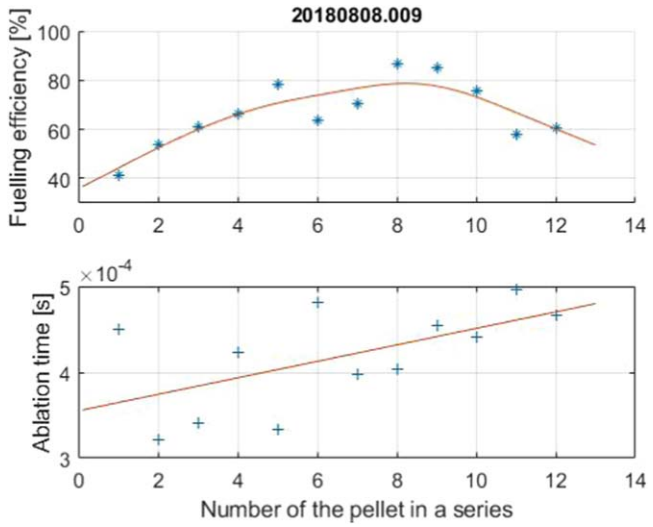

Figure 6. Upper plot: measured pellet fueling efficiency (*y*-axis, stars) versus pellet number (*x*-axis) within a series of 12 pellets injected into discharge 20180808.009 from the LFS. The solid line shows a spline fit to the data. The uncertainty of the data points is in the range of ±20% (see text above). Lower plot: pellet ablation time, normalized to pellet mass (*y*-axis, '+') versus pellet number. The solid line shows a linear fit to the data points.

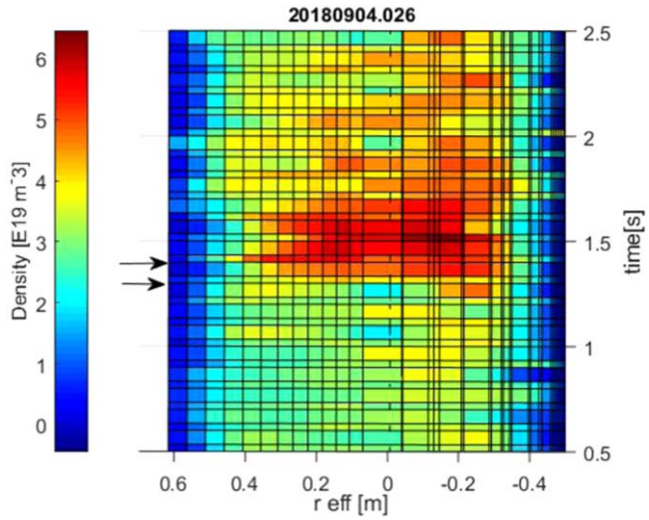

Figure 7. Thomson density profile development during a series of pellets for discharge 20180904.026. The *x*-axis shows the effective minor plasma radius, the *y*-axis the time. The two arrows indicate start and end of the series of pellets. The sidebar indicates the electron density in units of $10^{19}\,\mathrm{m}^{-3}$. The black horizontal lines indicate the Thomson laser times, no smoothing in direction of the time axis is performed. The black vertical lines indicate the Thomson measurement locations.

Even after short series of pellets, the electron density increase can be detected after a very short time in the plasma center, and peaked density profiles develop. This holds for both HFS and LFS pellets. Figure 7 shows as example of the temporal development of Thomson density profiles for a series of 5 pellets. The central density rises from $3 \times 10^{19}\,\mathrm{m}^{-3}$ to $6 \times 10^{19}\,\mathrm{m}^{-3}$ within 110 ms and decays soon afterwards. Throughout all discharges performed so far, the central electron density increases within a time scale of about several tens of ms during the series of pellets, and no considerable time delay can be observed between density rise and pellet injection times. These tens of ms are already long compared to the ablation time, but short compared to the particle confinement time. In figure 7 the two arrows indicate the beginning and end of the series of pellets. Within a time interval smaller than 30 ms after the last pellet, the highest density profile has developed. This corresponds to the time resolution of the Thomson scattering system.

One discharge example with very high density peaking is shown in figure 8 for shot 20171207.006. In this case, a series of 15 pellets raises the central density to a value of about $7 \times 10^{19}\,\mathrm{m}^{-3}$ (measured by Thomson scattering), while the profile shape changes from flat to strongly peaked. Here, the peaking factor is defined as the ratio of the central to the averaged electron density as measured by Thomson scattering. Each pellet can be seen as an upward step in the line density (solid line), with an average density increase of about $0.35 \times 10^{19}\,\mathrm{m}^{-3}$ per pellet. The series of pellets starts at 1.07 s and ends at 1.7 s. Prior to the pellet phase, the density peaking factor is about 1.2, a typical factor for discharges fueled with only gas puff. Next, the maximum density peaking of about 1.6 is reached at about 1.8 s, and remains peaked for roughly 0.5 s after the last pellet.

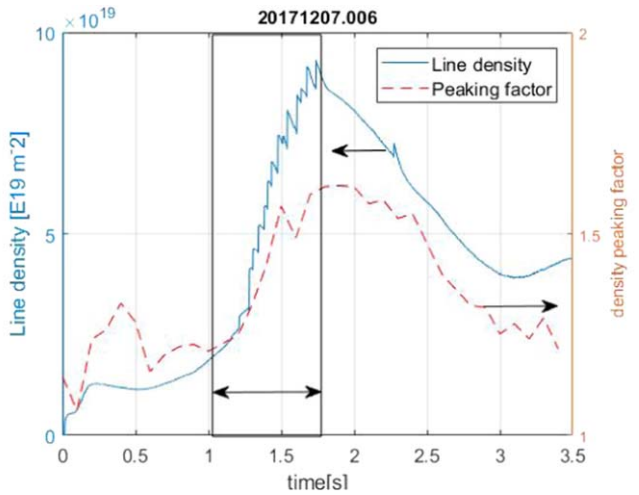

Figure 8. Time traces of the interferometer line integrated density (solid line, left *y*-axis) and the density peaking factor (dashed line, right *y*-axis) for discharge 20171207.006. The pellets are injected during the time period indicated by the double arrow.

Note that the decay of the line density after the series of pellets occurs with a half time in the range of ≈ 1 s, a typical value if no external gas puff is applied to the discharges. This is an indication that the particle confinement time and the particle diffusion time scale strongly exceeds the density profile development time, as observed in the discharges shown in the figures 7 and 8. This statement makes the assumption, that the particle transport does not change considerably during the series of pellets and that the wall recycling coefficient might be constant.

3.2. LFS/HFS comparison

A comparison between fueling efficiency achieved for pellets coming from HFS and LFS revealed no significant difference. Great care was taken to select discharges with constant heating power during the series of pellets for this comparison, and the integrated plasma radiation losses had to be significantly below the total heating power (below 30%). In addition, discharges were selected without external gas puff during the series of pellets, in order not to entangle the measured pellet fueling rates with particles coming from the gas feed. In total, 115 pellets could be identified which fulfill these requirements.

For that subset of pellets, the measured pellet fueling efficiencies are 70% ± 31% for LFS pellets and 88% ± 34% for the HFS pellets, in spite of the smaller HFS pellet masses. The deviations from the averages are not a measurement error in the statistical sense. Rather they show the limited shot-to-shot and pellet-to-pellet reproducibility of the experiments. In addition, the uncertainty for the evaluation of the pellet mass has to be kept in mind. Taking such scatter into account, the measured difference between the LFS and the HFS efficiency is obviously smaller than the attainable reproducibility of the experimental conditions.

It should be noted, however, that the mean value of efficiency for HFS is higher than for LFS. This indicates a slight advantage of HFS compared to LFS. Compared to tokamak results, the difference between HFS and LFS is, however, small. We assume that this small difference between HFS and LFS is a result of the comparably small *grad-B* term in W7-X, compared to tokamaks ($0.8\,\mathrm{T\,m^{-1}}$ for W7-X compared to $2\,\mathrm{T\,m^{-1}}$ for similar sized tokamaks). When considering HFS pellet injections for other stellarators or a reactor, one has to balance carefully whether the enhanced efforts (difficult port access on the inboard side, necessity of curved guiding tubes, etc) are worth such a comparably small gain.

When comparing directly the fueling efficiencies between the tokamak ASDEX-Upgrade (AUG) and W7-X, see [9], the most striking difference are the high LFS values in W7-X compared to <20% measured during H-mode discharges in AUG (see figure 3 in [9]). One reason for that difference might the strongly different shape of the n_e and T_e profiles, but also the underlying plasma transport and heating power density. In addition, for AUG the maximum pellet masses are assumed for calculation, whereas for W7-X the real pellet masses are taken into account. In W7-X, so far only L-mode discharges with ECRH could be maintained, with considerably different local transport parameters and a radial position of the steepest gradients deep inside the plasma, making a direct comparison difficult. Very positive for AUG is, however, the average improvement of the fueling efficiency by a factor of 4 when comparing HFS and LFS, in contrast to the much smaller ratio obtained in W7-X. In AUG, the HFS pellets penetrate deeper than the LFS pellets, an effect which was not observed in W7-X. Major obstacle for a direct comparison is the large average pellet mass difference in W7-X between HFS and LFS.

Pellet experiments performed from HFS and LFS in the heliotron LHD show a good agreement between the measurement and HPI2 code results [33]. These were the first experiments with HFS pellets in a helical device. However, here a comparison to W7-X is even more difficult than for AUG, because all plasmas are heated by a considerably amount of NBI, leading to an enhanced pellet ablation due to the high energetic heating ions. In LHD, typical fueling efficiencies are obtained in the range of about 50%, both for LFS and HFS. Comparable to W7-X, an outward displacement of the ablated pellet material is observed even for HFS pellets, presumably due to the magnetic hill structure in LHD. W7-X, in contrast, shows a slight magnetic well in the standard magnetic configuration. Future experiments in W7-X at higher plasma beta with deepened magnetic well will have to show, in how far the formation of this magnetic well might help for deeper deposition, both for HFS and LFS.

In order to investigate the pellet acceleration during ablation, fast video frames were taken at frame rates between 90 and 350 kHz. These investigations revealed a tokamak like behavior for LFS injected pellets: a clear outward drift of the pellet cloud [34] associated with a radial deceleration of the pellets caused by the asymmetric shielding of the drifting cloud [35] could be observed. These observations are more complex for HFS injected pellets: the pellet movies show that the pellet cloud drift tends to be an outward drift, too, although *grad*-B points towards the plasma center. In a few cases an inboard directed drift was also detectable.

The HPI2 code simulations partly confirm the experimental findings. HPI2 predicts no significant difference between HFS and LFS injections with regard to the depth of the ablation zone and the depth of the particle deposition. This is consistent with W7-X findings. However, HPI2 predicted in earlier investigations a considerably higher fueling efficiency for HFS compared to LFS [11], an effect which cannot be confirmed by the pellet experiments.

For the direct comparison between experiment and the HPI2 code, two well documented discharge sets were selected with comparable discharge parameters, one with LFS and one with HFS pellet injection. The experimentally determined pellet fueling efficiencies are 114% ± 54% for the HFS pellet discharges (including 15 pellets), and 66% ± 25% for the LFS discharges (including 31 pellets). As input for the HPI2 code, the plasma and pellet parameters of two representative discharge were chosen out of the mentioned sets, labeled 20180807.026 for the HFS case, and 20180807.027 for the LFS case. Figure 9 shows the results of the HPI2 calculations for these two cases. HPI2 predicts an inward drift of the ablated particles for the HFS case and an outward directed drift for the LFS case, as indicated by the radial distance between the maxima of the ablation and deposition profiles. The 95% reliability interval, resulting from a Gaussian process regression to the measured Thomson data points, indicates the uncertainty of the measurement. Note that this reliability interval is comparable or larger than the Thomson measurement error bars, however the latter are only statistical errors that take no possible systematic errors into account. The amount of density change (coming from the deposited

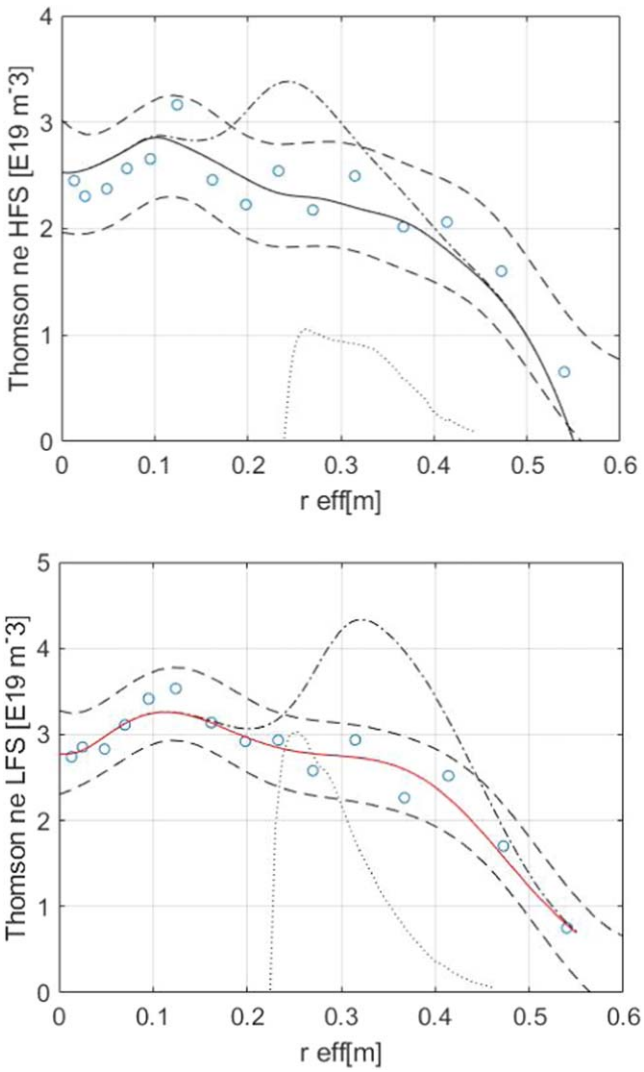

Figure 9. HPI2 code results for a HFS pellet case (upper plot) and a LFS case (lower plot). Density profiles as a function of the minor effective radius (*x*-axes). Experimental Thomson scattering data (circles), the HPI2 input profiles after spline smoothing (solid lines), HPI2 code results for the particle deposition (dotted–dashed) and pellet ablation (dotted). The dashed lines show the 95% prediction intervals (the interval of reliability of the fitted regression) to the experimental Thomson data after fit to a gaussian procedure regression.

particles) due to the pellets is comparable in size to that uncertainty, making a direct comparison between Thomson measurements and HPI2 calculations difficult. Therefore, only the Thomson burst-mode with its strongly enhanced time resolution might provide insight into the details of the deposition process. This holds in particular for the HFS case, where the pellets produce only a local density increase in the range of $1 \times 10^{19}\,\mathrm{m}^{-3}$. The situation is better for LFS pellets, where the density increase by a pellet is up to 2–4 times larger than the measurement uncertainty. This demonstrates, that even directly after a pellet (i.e. within a distance in time <10 ms after a pellet), no pronounced hollow density profiles can be detected with the standard Thomson system. Only the burst-mode Thomson scattering can reveal the slight hollowness of the density profiles directly after a pellet

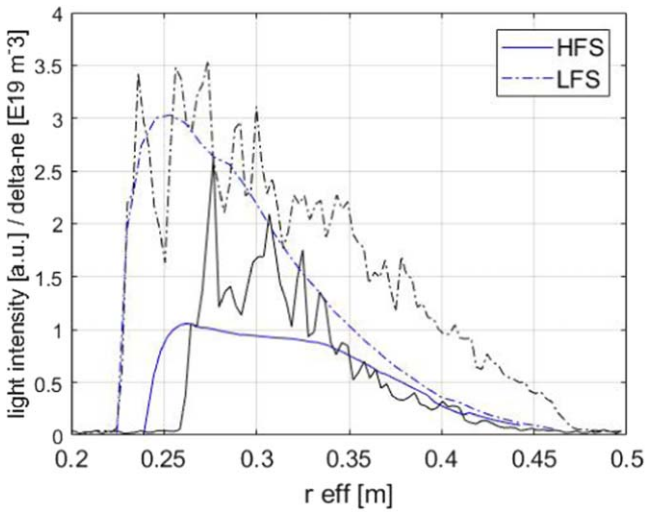

Figure 10. Measured pellet ablation light curves, plotted versus the minor plasma radius, for one HFS (black solid line) and one LFS pellet (black dotted–dashed line). The pellets enter the plasma from the right side. For comparison, the HPI2 results from figure 9 for the particle ablation are also shown again: HFS (blue solid line) and LFS (blue dotted–dashed line).

unambiguously, making the direct comparison between HPI2 code results and the standard Thomson scattering data impossible.

The HPI2 code predicts fueling efficiencies of 94% for the HFS case and 96% for the LFS case, hence the same values when taking the uncertainties of the input data into account. Within the measurement errors for the determination of the experimental fueling efficiencies, this is roughly consistent to the experiment.

Figure 10 shows measured filterscope ablation light curves for two pellets as indicated in figure 9 (for the HFS and the LFS), plotted as a function of the effective minor radius after taking into account the pellet speed and the local magnetic flux compression. It was assumed that the pellet's path of flight is straight without any deflection into poloidal or toroidal direction. Furthermore, a constant pellet speed has to be assumed. In addition, the HPI2 code results for the pellet ablation from figure 9 (dotted lines) are shown again for comparison in figure 10. As can be seen, the shapes of the light curves correspond very roughly to the predictions from HPI2, however not perfectly. The integral under the light curves correspond roughly to the amount of ablated pellet material as predicted by HPI2, and it is consistent to the measured pellet masses. For the HFS pellet, the total ablation depth is over-estimated by HPI2 by about 2.5 cm; a deviation which is certainly within the error margins for the profile data input for HPI2. In addition, the unreasonably high fueling efficiency of $>100\%$ for that pellet indicates that the measured HFS pellet mass (as input for HPI2) was probably estimated inexactly. For the LFS pellet, the shapes of the curves match very well, albeit the local ablation rate in the outer part of the plasma (i.e. for $r_{\mathrm{eff}} > 0.3$ m) seems to be slightly under-estimated by HPI2, or it is slightly over-estimated by the filterscope light intensity.

Table 1. Pellet fueling efficiencies for X2/O2-mode ECRH and LFS/HFS pellet injection. The uncertainties are the standard deviation, assuming only a statistical error. In total, 135 individual pellets are taken into account.

	X2-mode ECRH	O2-mode ECRH
LFS pellet injection	77% ± 14%	71% ± 12%
HFS pellet injection	88% ± 11%	87% ± 8%

Experiments were performed with X2-mode and O2-mode ECRH, both with LFS and HFS pellet injection. The idea was to tailor discharges with more peaked T_e profiles (for the case of X2-mode ECRH) in contrast to more flat T_e profiles (for the case of O2-mode ECRH) because of the lower single-pass absorption with O2-mode heating, and thus, a broader power deposition zone inside the plasma. The steeper gradient in T_e might result in an enhanced outward directed particle thermo-diffusion for the particles, deposited after pellet injection. In addition, it is suspected that a broader power deposition zone might produce a suprathermal electron population close to the plasma edge, which might influence the pellet ablation or particle deposition. In order to investigate that possible influence, the pellet fueling efficiencies are compared for these four combinations, table 1 shows the results. Note that the standard deviation, as shown in the table, does not take into account the systematic uncertainty that is higher (namely the 20% mentioned above), because only the statistical measurement scatter is considered.

The data show no significant difference between X2 and O2-mode ECRH, indicating no impact of the broadening of the ECRH power deposition zone on the pellet fueling efficiency. As above, however, a difference in the mean values of LFS and HFS injection is visible, although being smaller than the uncertainties. Figure 11 shows two T_e profiles of the discharges with pellet injection and X2/O2-mode ECRH power deposition, but otherwise comparable plasma parameters, as used for the evaluation shown in table 1. The T_e profiles show temperature gradients of 11.0 keV m^{-1} for the O2-mode case and 14.1 keV m^{-1} for the X2-mode case, in the central part of the plasma. Nevertheless the pellet fueling efficiencies show no significant difference. This indicates only marginal (or no) impact of the electron temperature or possible suprathermal electrons, produced by the ECRH, on the fueling efficiency. This is supported by the observation, that during the OP1.2 campaign no distinctive hollow density profiles could be observed, independent of the broadening of the ECRH power deposition zone. The Thomson data are taken about 1 s prior to the pellet injection, with very stable and constant discharge conditions between the Thomson time and the time of pellet injection.

3.3. Series of pellets

In accordance with previous experiments in LHD, the concept of the injection of series of pellets works also in W7-X. Although the ablation depth of the pellets is restricted to regions in the outer half of the minor plasma radius, central fueling could always be observed. As already observed in LHD, the fueling efficiency increases with the number of pellet within a series, until a maximum is reached. For additional pellets, the efficiency drops again. In LHD discharges, about 4–5 pellets were the maximum needed to sustain stable discharges; for longer series of pellets the discharges risked to be terminated prematurely. This is partly due to the fact that the hydrogen pellets in LHD (3.0 and 3.4 mm in the pipe-gun) are much larger than the pellets in W7-X (2 mm in the blower-gun). In both machines, a trend for deeper penetration of later pellets in a series is observed compared to earlier ones in the same series.

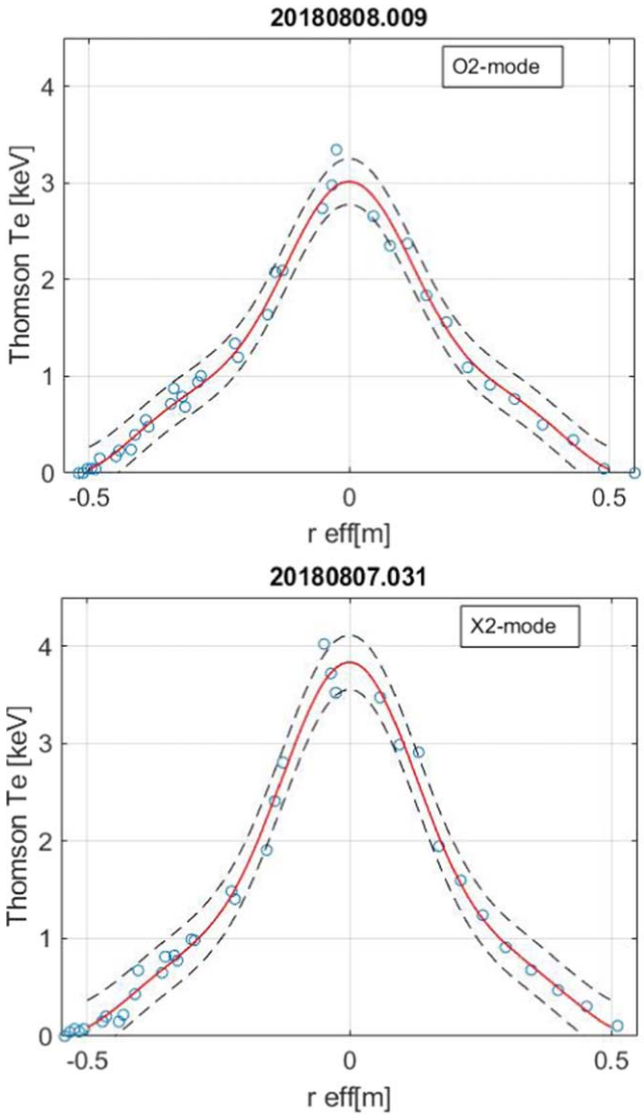

Figure 11. Thomson scattering T_e profiles (circles) for O2-mode ECRH (upper plot, discharge 20180808.009) and X2-mode ECRH (lower plot, discharge 20180807.031). The solid lines show a fit of the measurement to Gaussian process regression model, being used in this case because it conserves well the value of the T_e gradients and takes the point-by-point scatter better into account for the estimate of the uncertainty. The dashed lines show the upper and lower boundaries of the 95% prediction intervals (the interval of reliability of the fitted regression). Negative effective radii (r_{eff}) are on the inboard side, positive on the outboard side. A symmetric T_e profile function is assumed for the fit.

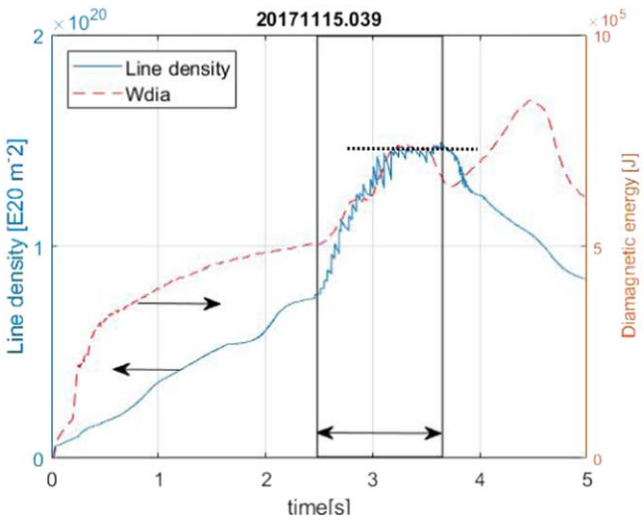

Figure 12. Time traces for discharge 20171115.039. Shown are the interferometer line density (left *y*-axis, solid line) and the diamagnetic energy (right *y*-axis, dashed line). The pellet injection phase is indicated by the vertical lines with the double arrow. The dotted line indicates the flat-top phase.

In the W7-X experiments reported here stationary hollow density profiles, as might result from the local particle deposition close to the plasma edge, have not been observed during the pellet injection phase. In contrast, in LHD such cases were observed. A small number of discharges with fast density re-distribution could be observed, turning hollow into peaked profiles on a time-scale faster than allowed by diffusion. In W7-X such a strong transient effect was never observed, since the density profiles tend to be fueled centrally, from the beginning of the pellet series (see figure 7 for instance).

In W7-X, only one pellet-fueled discharge ended by a radiative collapse has occurred to date, in contrast to LHD where several discharges ended in a collapse or a temperature-hole scenario [36] after an extended series of pellets. Radiative density limit studies in W7-X [37] reveal upper critical average densities for gas puff fueled discharges. Impurity radiation, i.e. radiative power losses, seem to be decisive for the observed density limit. The above mentioned pellet discharge exceeded the density limit (as published in [37]) for discharges with gas-puff by a factor of about 2.5. Further experiments will be needed to confirm, whether the upper density limit with pellet fueling can be pushed towards higher density values, compared to gas puff fueled discharges.

For very long series of pellets in W7-X, the trend to stationary pellet particle fueling rates can be observed. This scenario is promising for sustaining stationary discharges in future campaigns, where the steady-state pellet injector will be available to provide a continuous series of pellets. This minimizes the risk of a premature plasma collapse. Figure 12 shows an example of such a discharge, fueled with a series of 33 pellets. The entire stockpile of the blower-gun was emptied. After about 3 s, a stable discharge phase is reached with, to some degree, stationary plasma parameters. The central Thomson electron densities reach $1.4 \times 10^{20}\,\mathrm{m}^{-3}$ for about 600 ms. Next, at about 4.5 s, a phase of improved energy confinement follows the pellet series.

4. Discussion, outlook

Central particle fueling in the stellarator W7-X has been performed successfully with series of pellets, even with a penetration of pellets of only about 40% of the minor plasma radius. Regardless of the heating scenario or the magnetic configuration, fueling efficiencies higher than 70% on average could be achieved. So far, there was no necessity for the mitigation of hollow density profiles by pellets. However, since future experimental campaigns in W7-X will focus on the attainment of neoclassical transport, this might become an essential issue. While we in general did not see hollow density profiles on W7-X, we were able to peak up flat profiles at least transiently, by doing pellet injection. Even if the pessimistic predictions for inherent outward particle diffusion by off-diagonal transport for the latter can be confirmed [3], the envisaged central particle fueling rates by pellets will be high enough to compensate.

The future steady-state pellet injector under development for the W7-X is specified to operate at 10 Hz repetition frequency with cylindrical pellets of 3 mm length and diameter, containing 1.1×10^{21} protons (for hydrogen ice). Given the numbers cited above of 70% plasma fueling efficiency for LFS injection geometry, and 60% for the guide tube, this provides a central fueling rate of 4.6×10^{21} protons s^{-1}, exceeding the neoclassically predicted required flux of 10^{21} particles s^{-1}.

Long series of pellets with more than 30 pellets could be successfully performed to reach central densities of up to $1.4 \times 10^{20}\,\mathrm{m}^{-3}$ with O2 mode ECRH heating. Such a high-density phase could be kept stationary for about 600 ms (corresponding to about 4 energy confinement times). This demonstrates the capability of pellet injection, to reach and maintain high density phases. Record fusion triple products for a stellarator of up to $0.65 \times 10^{20}\,\mathrm{keV\,m}^{-3}$ s could be reached [38] during the last campaigns with pellets. This confirms the expectation, that high densities provide good energy confinement, in accordance with the positive exponent of the ISS04 density scaling.

However, in order to maintain the plasma parameters during stationary high density phases as constant as possible, it is considered that the large 3 mm pellets of the specified steady-state injector might be too large, in some cases. In particular, in the vicinity of the ECRH cut-off density, overly large pellets might violate this density threshold occasionally. Therefore, the present planning foresees the technical option to vary the pellet size between 2 and 3 mm by choice, and to vary the pellet repetition frequency between 10 and 20 Hz. Future technical tests of the steady-state system will reveal, to what extent the vacuum pump systems and the guide tube with its poor gas conductivity will be able to sustain more stable injector conditions with these parameters during continuous pellet injection.

We were able to demonstrate central particle fueling with short delay times between the pellet ablation at the plasma edge, and core density increase. This confirms the capability

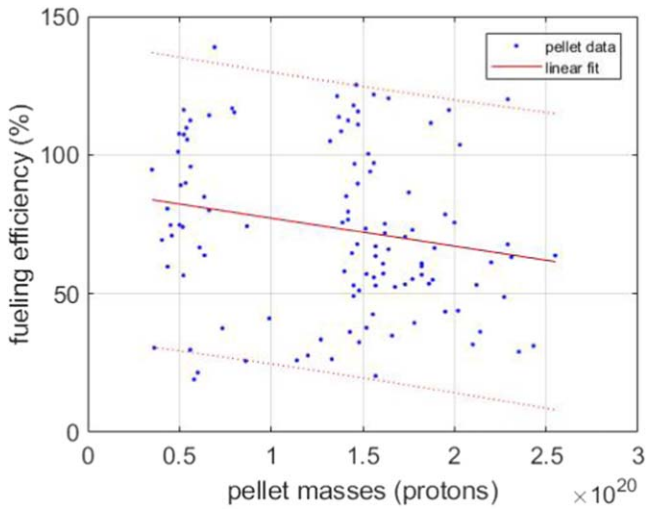

Figure 13. Result of the linear regression between fueling efficiency and pellet mass. The dots show the experimental data, the solid line the regression, the dotted lines the 90% prediction bounds for the regression. Fueling efficiencies >100% are unrealistic and therefore due to the measurement uncertainty.

to fuel W7-X plasmas centrally with pellets, even if the pellets are comparably small and slow.

A possible impact of supra-thermal electrons, produced by ECRH, on the pellet ablation and particle deposition, could not be observed. The experimental findings for the pellet ablation are conform to HPI2 code calculations without supra-thermal electrons. This indicates that the ablation process in W7-X appears unaffected.

Only ECRH heated discharges were performed during the last two experimental campaigns with pellet injection. All these discharges are expected to show a more or less pronounced supra-thermal electron population. No NBI only heated discharges with pellets were realized for comparison (i.e. certainly without any supra-thermal electron population), so far. This point therefore remains an open issue for the future, in particular for the assessment of pellet fueling in long discharges with pure ECRH. An enhanced particle deposition after pellet injection in the presence of supra-thermal electrons in the plasma core [39] cannot be supported, so far, due to the same reason.

The comparison between LFS and HFS revealed, within the scatter of data points, a slightly enhanced fueling efficiency for HFS compared to LFS. The enhancement is smaller than the experimental uncertainty of the data points. It could be suspected that the comparison between HFS and LFS pellets is corrupted because of the systematically smaller HFS pellets, but a linear regression analysis between the experimental pellet masses and fueling efficiencies does not support this suspicion. Figure 13 shows that result for all pellets that were used for the evaluation of the efficiency. The fueling efficiency is no function of the pellet mass, within the statistically significant prediction bounds for the regression.

Therefore, the technically much simpler solution of LFS launch will be realized for future campaigns, avoiding the problems posed by a curved and long guide tube passing through the machine center to the inboard launch site. LFS provides the possibility to use a straight guide tube with only minimal bends, thus allowing for higher pellet speeds and hence deeper penetration. The steady-state injector can thus be projected to pellet velocities well above 1 km s^{-1}.

The outward drift of the pellet material, as predicted by HPI2 for LFS pellets, could be confirmed experimentally. However, it is not understood why no clear inward drift for HFS pellets, as predicted by HPI2, is seen by the fast camera system. The small observed difference in fueling efficiency between HFS and LFS pellets, however, is consistent with that obviously missing inward drift for HFS pellet material.

As no HFS pellet experiments will be possible in the next campaigns in W7-X, other strategies for a better understanding are welcome. One might be the attempt to take advantage of a deepened magnetic well due to the diamagnetic effect in high plasma pressure (high beta) discharges, that might promote deeper fueling compared to low-beta plasmas because of the stronger inward directed *grad-B*. Purely NBI heated discharges at lowered magnetic field could be conducted for that purpose because here beta is increased due to the smaller magnetic field strength. ECRH in X2 and O2 polarization at lowered magnetic field is not possible because the 140 GHz is resonant only at 2.5 T. An alternative to pure NBI might be resonant ECRH in X3 polarization and with 1.66 T magnetic field strength. A variation of the magnetic configuration alone might not be helpful, as the average *grad-B* does not vary considerably over the range of possible magnetic configurations.

The technique of series of pellets works well on W7-X. Even the small and slow pellets can obviously benefit from plasma cooling by earlier pellets in a series, helping later pellets to penetrate deeper and to fuel better. This technique will help in the future for the sustainment of long ECRH discharges with X2 mode heating, as too strong transient density increases by overly large pellets can be avoided, which might otherwise transiently violate the cut-off density. For ECRH in O2 mode heating the transient cooling effects by overly large pellets are mitigated. These findings are supported by successful earlier experiments in LHD, where series of relatively slow and small pellets enabled access to high-density, steady-state discharges with improved global energy confinement [40]. A sufficiently low edge density, low wall recycling and low neutral gas pressure are considered as decisive clue towards improved discharges at high central density.

Presently, several hypotheses are discussed, for which mechanisms might be responsible for the transient increase of the energy confinement after the series of pellets. Within the scope of this paper we only can conclude, that central particle fueling, density profile peaking and improved energy confinement correlate. Some of the properties of these discharges resemble to various modes of improved confinement, as observed in other machines [41]. Narrow and peaked density profiles with enhanced density gradients over the entire minor radius might help stabilizing ion temperature gradient modes transiently [42]. The transient peaking of the density profiles resembles the pellet enhanced performance mode [43] as

discovered in the tokamak JET. There, reduced ion transport correlated with density peaking was observed. In the heliotron CHS, and in other helical machines, the reheat-mode [44] could be observed, with a considerable improvement of the confinement and peaked density profiles, in particular directly after terminating the external gas puff. In opposite to the reheat-mode, the improved energy confinement in W7-X appears only after the end of series of pellets. Frequently, the improved confinement phase in W7-X is accompanied by strong negative radial electric field values, probably supported by the high central ion temperature [45]. A comparable behavior in the heliotron LHD, i.e. a phase of improved energy confinement after a series of pellets, is described in [46]. The future analysis will have to show, whether the same physics is underlying in W7-X.

As the future steady-state injector will be rather large, complex and expensive, the use of the blower-gun was a very helpful opportunity to learn about the requirements of W7-X well in advance. Several lessons concerning pellet size and repetition frequency were learned, and some aspects for the optimization of the steady-state injector could be adapted at an early planning stage into the design. The present design of the steady-state injector foresees the injection of pellets with 3 mm size, with a fixed repetition frequency of 10 Hz. However, as smaller pellets with higher repetition frequency were used successfully, we will strive for a modification of the design. In addition, for the future a smart pellet triggering scheme is considered which might allow for density feedback control, or even the feedback stabilization of the density profile shape, so as to maintain an improved energy confinement scenario.

Acknowledgments

This work has been carried out within the framework of the EUROfusion Consortium and has received funding from the Euratom research and training programme 2014–2018 and 2019–2020 under grant agreement No. 633053. The views and opinions expressed herein do not necessarily reflect those of the European Commission.

We gratefully acknowledge the support of IPP Garching, Germany, in particular for loaning us the blower-gun. The ASDEX-Upgrade pellet team (M Beck, P Lang, B Ploeckl, W Weisbart) configured the injector according to our requirements. M Dibon tested the prototypes of curved guide tubes and characterized the blower-gun performance in detail.

ORCID iDs

J Baldzuhn https://orcid.org/0000-0001-5667-351X
K McCarthy https://orcid.org/0000-0002-5881-1442
S A Bozhenkov https://orcid.org/0000-0003-4289-3532
A Langenberg https://orcid.org/0000-0002-2107-5488
T S Pedersen https://orcid.org/0000-0002-9720-1276
G Schlisio https://orcid.org/0000-0002-5430-0645
E R Scott https://orcid.org/0000-0002-1389-1151
G Wurden https://orcid.org/0000-0003-2991-1484

References

[1] Grieger G *et al* 1992 *Phys. Fluids* B **4** 2081
[2] Beidler C D *et al* 2018 *Plasma Phys. Control. Fusion* **60** 105008
[3] Maassberg H, Beidler C D and Simmet E E 1999 *Plasma Phys. Control. Fusion* **41** 1135
[4] Sardei F 1991 *Proc. 18th EPS Conf. Control. Fusion Plasma Phys. part II (Berlin)* p 193
[5] Karulin N E 1994 Transport modelling of stellarators with ASTRA *IPP Report* 2/328 Max-Planck Institute for Plasma Physics
[6] Greenwald M 2002 *Plasma Phys. Control. Fusion* **44** R27–80
[7] Yamada H *et al* 2005 *Nucl. Fusion* **45** 1684
[8] Lang P T *et al* 2018 *Nucl. Fusion* **58** 036001
[9] Lang P T *et al* 1997 *Phys. Rev. Lett.* **79** 1487
[10] Pégourié B *et al* 2005 *Plasma Phys. Control. Fusion* **47** 17
[11] Panadero N *et al* 2018 *Nucl. Fusion* **58** 026025
[12] Takeiri Y *et al* 2017 *Nucl. Fusion* **57** 102023
[13] Klinger T *et al* 2017 *Plasma Phys. Control. Fusion* **59** 014018
[14] Bosch H S *et al* 2017 *Nucl. Fusion* **57** 116015
[15] Wolf R C *et al* 2017 *Nucl. Fusion* **57** 102020
[16] Pedersen T S *et al* 2017 *Phys. Plasmas* **24** 055503
[17] Wolf R *et al* 2019 *Plasma Phys. Control. Fusion* **61** 014037
[18] Pedersen T S *et al* 2018 *27th IAEA Fusion Energy Conf. (Ahmedabad, India)*
[19] Dibon M 2014 Entwicklung und verbesserung eines blower gun pellet injektors für die anwendung in thermonuklearen fusionsanlagen *Master-Thesis* Technical University Munich, Max-Planck Institut IPP
[20] Combs S K, Caughman J B O and Wilgen J B 2006 *Rev. Sci. Instrum.* **77** 073503
[21] Kocsis G *et al* 2015 *Fusion Eng. Des.* **96–97** 808
[22] Damm H 2018 Upgrade of the wendelstein 7-X thomson Scattering diagnostic to study short transient plasma effects —a demonstration on pellet injection for stellarator fueling (IPP 2018–13) *Master-Thesis* Garching: Max-Planck-Institut für Plasmaphysik (https://doi.org/10.17617/2.2596741)
[23] Pasch E *et al* 2016 *Rev. Sci. Instrum.* **87** 11E729
[24] Bozhenkov S A *et al* 2017 *J. Instrum.* **12** P10004
[25] Bozhenkov S A *et al* 2013 *Fusion Eng. Des.* **88** 2997
[26] Hoefel U *et al* 2019 *Rev. Sci. Instrum.* to be published
[27] Langenberg A *et al* 2018 *Rev. Sci. Instrum.* **89** 10G101
[28] Brunner K J *et al* 2018 *J. Instrum.* **13** P09002
[29] Zhang D *et al* 2010 *Rev. Sci. Instrum.* **81** 10E134
[30] Winters V *et al* 2018 *45th EPS Conf. Plasma Physics (Prague, Czech Republic)*
[31] Baldzuhn J *et al* 2018 *Plasma Phys. Control. Fusion* **60** 035006
[32] Dibon M *et al* 2015 *Fusion Eng. Des.* **98–99** 1759
[33] Matsuyama A *et al* 2012 *Nucl. Fusion* **52** 123017
[34] Kocsis G *et al* 2018 *45th EPS Conf. Plasma Physics (Prague, Czech Republic)*
[35] Szepesi T, Kálvin S, Kocsis G, Lang P T, Senichenkov I and ASDEX Upgrade Team 2009 *J. Nucl. Mater.* **390–391** 507
[36] Nakamura Y *et al* 2017 *Nucl. Mater. Energy* **12** 124
[37] Fuchert G *et al* 2018 *45th EPS Conf. Plasma Physics (Prague, Czech Republic)*
[38] Pedersen T S *et al* 2019 *Plasma Phys. Control. Fusion* **61** 014035
[39] McCarty K *et al* 2018 *Plasma Phys. Control. Fusion* **61** 014013
[40] Sakamoto R *et al* 2006 *Nucl. Fusion* **46** 884
[41] Wagner F 2017 *Eur. Phys. J.* H **43** 523

[42] Alcusón J A, Xanthopoulos P, von Stechow A and Grulke O 2018 *23rd Joint EU-US Transport Task Force Meeting (Seville, Spain)*

[43] JET Team 1988 *Proc. 12th Int. Conf. on Plasma Physics and Controlled Nuclear Fusion Research* vol 1 *(Nice, 1989)* (Vienna: IAEA) p 215

[44] Morita S *et al* 1992 *Proc. 14th Int. Conf. on Plasma Physics and Controlled Nuclear Fusion Research* vol 2 *(Würzburg, 1993)* (Vienna: IAEA) p 515

[45] Pablant N A *et al* 2018 *27th IAEA Fusion Energy Conf. (Ahmedabad, India)*

[46] Ohyabu N *et al* 2006 *Phys. Rev. Lett.* **97** 055002